Received: 10 May 2019 | Revised: 10 September 2019 | Accepted: 16 September 2019

DOI: 10.1002/ese3.502

RESEARCH ARTICLE

Energy Science & Engineering Open Access

Ceramic high temperature plate-fin heat exchanger: A novel methodology for thermomechanical design investigation

Jürgen Haunstetter | **Volker Dreißigacker**

Institute of Technical Thermodynamics, German Aerospace Center, Stuttgart, Germany

Correspondence
Jürgen Haunstetter, Institute of Technical Thermodynamics, German Aerospace Center, Pfaffenwaldring 38-40, Stuttgart, Germany.
Email: juergen.haunstetter@dlr.de

Abstract

The basic methodology of a novel, time-saving approach for critical thermomechanical design studies of ceramic high temperature plate-fin heat exchanger is presented. This approach allows the determination of local displacements, by applying the outer heat exchanger boundary conditions on a substitute model. These displacements are then used for detailed calculation of local stresses. The methodology is based on the effective Young's modulus, effective shear modulus, and effective Poisson ratio. Simulation models have been developed to determine these effective substitute properties. A model verification has been performed with a compression test rig. The simulation predicts the experimental results with deviations below 3%, which proves the feasibility and reliability of the effective material models. In order to reduce the parametric effort of the substitute simulation model, information about the material behavior is important. Here, the results indicate an orthotropic material behavior of the fin structure. This reduces the independent substitute material properties required for the characterization of the substitute model, which also reduces the overall simulation time.

KEYWORDS

ceramic plate-fin heat exchanger, effective material constants, high-temperature heat exchanger, OSF heat exchanger, substitute material properties, substitute model

1 | INTRODUCTION

Whenever metallic heat exchanger exceeds their maximum operating temperature and chemical limits, ceramic materials offer an alternative solution in high temperature applications. For industrial processes with temperatures above 900°C such as glass, ceramics, or metal production, ceramic heat exchangers can raise the maximum temperature limit for waste heat recovery and thus lead to higher efficiencies. Further promising applications include externally fired gas turbines, which use alternative fuels like concentrated solar power or biomass as a thermal power source.[1-3]

Different studies on ceramic heat exchanger technology are available from literature. A review of the state of the art of ceramic heat exchangers and their applications, including primary heat exchangers in gas-fired furnaces, recuperators and heat exchanger usage in the chemical industry, is given by Sommers et al.[4] The study focuses on ceramic microchannel and plate-fin heat exchangers. Their advantages are high exchanger surface to volume ratio, compact structure, and high efficiency compared with other ceramic heat exchanger types like heat-pipes. Design and optimization studies of those ceramic plate heat exchangers are mostly based on flow distribution, thermal performance, and pressure drop behaviour.[5-7]

A special microchannel design is the offset strip fin (OSF) design. Schulte-Fischedick et al[8] transferred it from metallic plate heat exchangers to ceramic plate heat exchangers. He presented the thermal design and manufacturing process of a sintered silicon carbide high temperature heat exchanger (HTHE) for power plant application. An experimental investigation on thermal performance and pressure drop performance of a sintered silicon carbide OSF heat exchanger prototype was performed by Haunstetter et al.[9] He conducted tests at temperatures up to 800°C and pressures up to 5 bar and compared the results with correlations from literature. CFD-simulation studies on thermal performance and pressure drop as well as experimental tests of an OSF ceramic plate heat exchanger made from alumina (Al_2O_3) were carried out by de Mello et al.[10-12] The HTHE was operated at temperatures up to 800°C and ambient pressure conditions. However, structural failure was observed resulting from thermal-induced stresses at high temperatures.

This shows that in addition to thermal and pressure loss investigations, there is also the necessity for thermomechanical design studies. This is due to the usually ionic or covalent atom bonding of ceramics, which results in a brittle material behavior, leading to high risks of mechanical integrity for a lifetime of 20 years. Studies on ceramic thermo-structural analysis for different ceramic components are already available from literature.[13-16] However, there is a lack of thermomechanical considerations of ceramic heat exchangers. Smyth[17] discussed challenges of thermal stress prediction and control within ceramic heat exchangers and their ability to withstand thermal cycling. Detailed thermo-structural design investigations for an OSF ceramic plate HTHE were performed by Schulte-Fischedick et al.[8,18] They evaluated a small core and distributor section by assuming the maximum stresses in areas with highest temperatures; external stress influences were not considered. Nevertheless, outer boundary conditions like pipe connections or press fit fixations and the overall temperature profile are of significant importance for the deformation behavior of the whole heat exchanger. They lead to increased internal deformation and stresses, especially shear stresses. Thus, for the identification of low-stress designs and areas of critical stresses, the whole heat exchanger arrangement, consisting of process connection, distributor, and heat exchanger core (fin structure), needs to be modeled in detail.

However, complete and detailed thermomechanical design investigations of microchannel and plate-fin heat exchangers are related to extensive computational effort due to the filigree internal structure, which usually consists of a large number of fins with numerous geometrical degrees of freedom. Therefore, in this paper, we introduce a novel methodology to reduce the calculation effort and to allow wide parameter variation studies. The methodology is based on the formulation and implementation of a homogenized substitute model, which will be formulated and implemented in finite element method (FEM) software. This approach yields similar body displacements compared with a detailed model. By transferring these space-dependent displacements into the detailed structure, the local stresses in the heat exchanger geometry can be evaluated. A fundamental step for this methodology consists in the homogenization of the detailed filigree internal structure, which is done with so-called effective material properties. Therefore, simulations are conducted and validated based on experimental results in order to identify the material and geometry-dependent parameters and to determine the global mechanical material behavior.

The purpose of this article is to provide the basis for simplified thermomechanical design studies of ceramic plate-fin heat exchangers. First, the methodology is described in Section 2. The numerical models and determination of effective substitute material parameters are presented in Section 3. In Section 4, the experimental setup for the shear modulus verification is explained and illustrated. The results are visualized and discussed in Section 5. The conclusion follows in Section 6.

2 | METHODOLOGY

Basically, the here presented methodology can be applied to various heat exchanger designs. Here, it is applied to a ceramic microchannel plate-fin heat exchanger with an OSF core (Figure 1). This structure allows low-stress design solutions, high heat transfer rates, and an internal tightness between two heat transferring fluids due to its sintered monolithic structure. In addition, the design has a mechanical support function, which is provided by its fins. They support against internal pressure differences between the two fluid

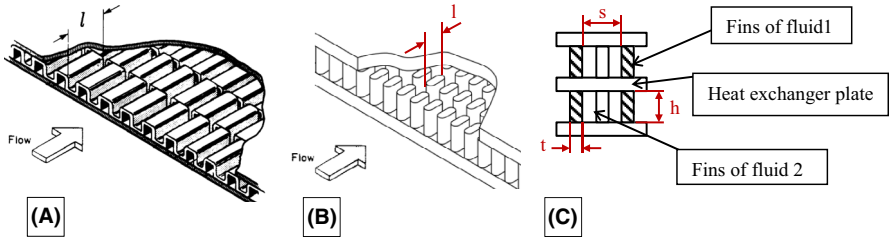

FIGURE 1 Graphical representation of a typical metallic offset strip fin core (A) and a ceramic OSF heat exchanger plate (B) with characteristic geometric dimensions (C)[21]

streams and lead to a stabilization effect to resist outer pressure impingements.[8]

Nevertheless, thermomechanical design simulations are necessary for the identification of mechanical stable arrangements. However, due to the large number of fins and the numerous geometrical degrees of freedom such as fin length (l), height (h), thickness (t), and spacing (s), these calculations require extensive computational effort. For this purpose, an alternative approach is developed, which is illustrated in Figure 2.

The basic idea is to use a homogenized substitute heat exchanger model. This requires effective mechanical substitute material properties consisting of the effective Young's modulus E, effective shear modulus G, and effective Poisson ratio v. Those are determined from a small symmetric section of the heat exchanger core through standardized test procedures implemented in ANSYS® mechanical 18.1 and serve as fundamental set for the homogenized substitute model. The model itself shows the same geometric dimensions as the real HTHE, but without any fins and spaces in its core. After imprinting external boundary conditions, such as temperature curves and forces, the substitute model leads to comparable body displacements as a detailed HTHE model. The resulting local displacements are then transferred to the detailed fin structure model to determine critical local stresses. In addition, the material behavior of the symmetric fin section is taken into account when determining the effective substitute material properties. The reason for this is the nonisotropic behavior of the symmetric fin profile, which is due to its porous structure and leads to direction-dependent material properties. A complete anisotropic structural material behavior requires, according to the stress-strain relationships, 21 independent constants. These constants have to be defined in a 3D calculation in ANSYS®. If the internal defects or reinforcements are evenly distributed, the required material constants can be reduced. By proving orthotropic behavior of the symmetrical fin section model, only nine independent constants are required, making simulation studies more time-efficient.

3 | MODELING

For parametrization of the homogenous substitute model, three effective material constants are required, including the effective Young's modulus, Poisson ratio, and shear modulus.

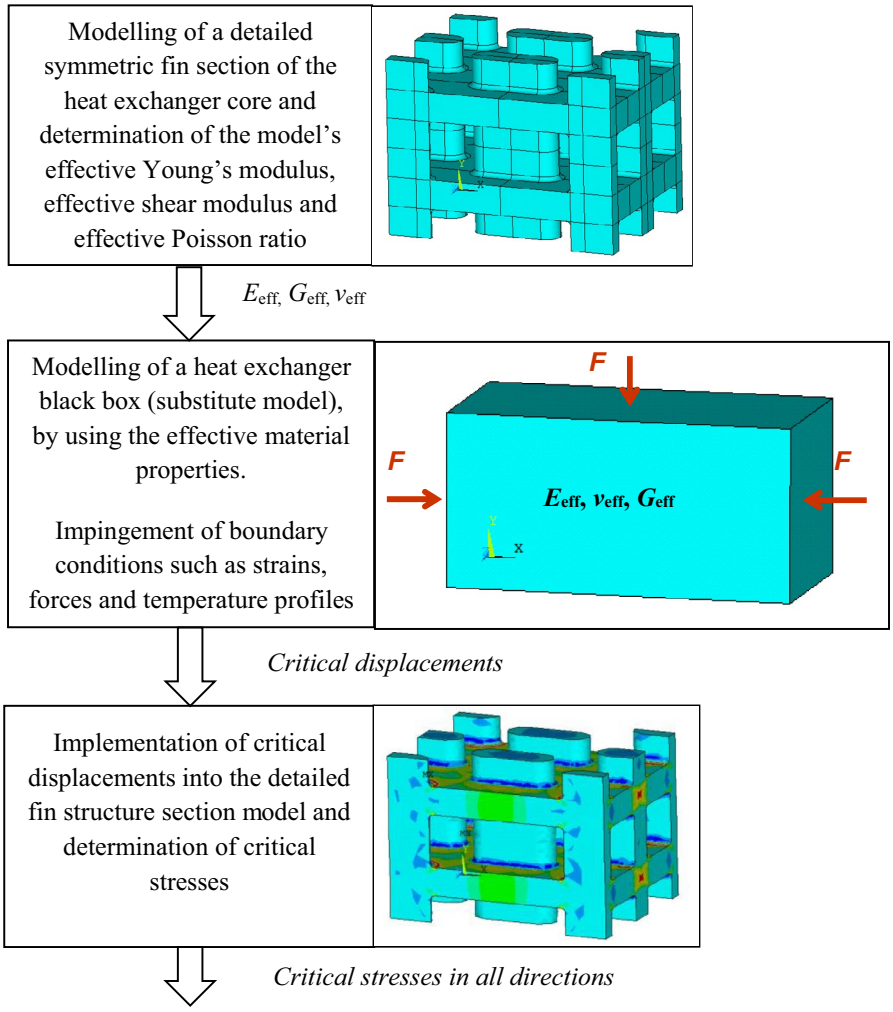

FIGURE 2 Schematic flow sheet of novel stress determination

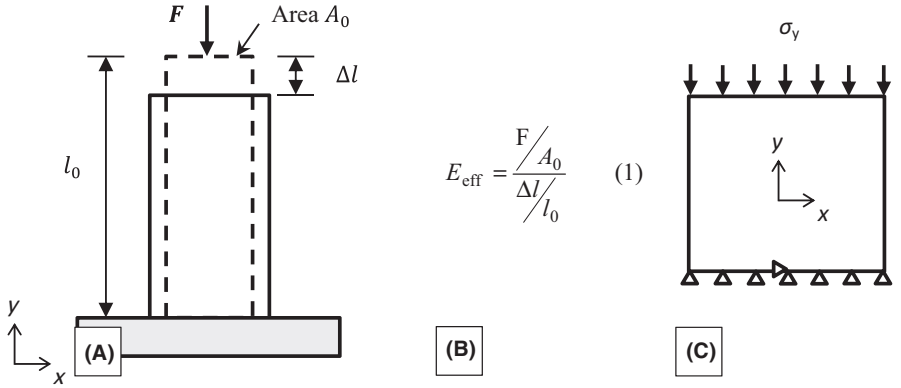

FIGURE 3 Schematic representation of a compression test (A), the linear relation of Young's modulus (B), and the FE model for E_y determination in simplified 2D illustration (C)[22]

Those are determined through standardized test procedures as described by the German Industrial Standard (DIN), using FEM simulations with ANSYS® mechanical 18.1.

3.1 | Effective Young's modulus

The Young's modulus is defined as the stress-strain ratio of a sample when a predetermined force is induced. A well-known method for determining the Young's modulus is a so-called compression test. The sample has a fixed bearing at one end, whereas a perpendicular force is impinged the other end. Simultaneously, the change in length is measured. The Young's modulus is calculated by using the linear relation given in Equation (1) (Figure 3B). This linear elastic behavior is typical for most metals and for brittle materials such as ceramics. A schematic representation of the compression test is illustrated in Figure 3A.

For fiber composite or porous materials, the effective Young's modulus is anisotropic, resulting in different Moduli for *x*-, *y*-, and *z*-direction. As the fin structure can be considered as a porous material, a calculation for each direction has to be carried out to determine E_x, E_y, and E_z.[19] This is shown schematically in Figure 3C, where as an example and for better visualization the FE model for effective Young's modulus determination in *y*-direction (E_y) is depicted as a 2D rectangle model instead of a 3D OSF structure. For the calculation of E_x and E_z, the procedure is similar, except for the position and direction of the boundary conditions. To determine E_x, the bearing and stress must be set in *x*-axis direction and for E_z in *z*-axis direction.

3.2 | Effective Poisson ratio

The Poisson ratio is defined as the ratio of lateral strain to longitudinal extension (Equation 2 in Figure 4B) of a sample when a defined uniaxial force acts on it. The Poisson ratio can be determined either by a compression or by a tensile test. The latter is implemented in ANSYS®. The fixed bearing is attached opposite the acting force. For example, an elongation in *y*-direction takes place, which leads to a length reduction in *z*- and *x*- direction. v_{yx} and v_{yz} can be determined according to Equation (2). These ratios describe the strain in *x*- or *z*- direction, while a force acts parallel to the *y*-axis. A simplified 2D representation of the FE model with the boundary conditions is shown in Figure 4C.

Due to the anisotropic effective Young's modulus (*x*, *y*, and *z*-axis) and the associated variation in elongation, six effective Poisson ratios can be differentiated (v_{xy}, v_{xz}, v_{zx}, v_{zy}, v_{yx}, and v_{yz}).

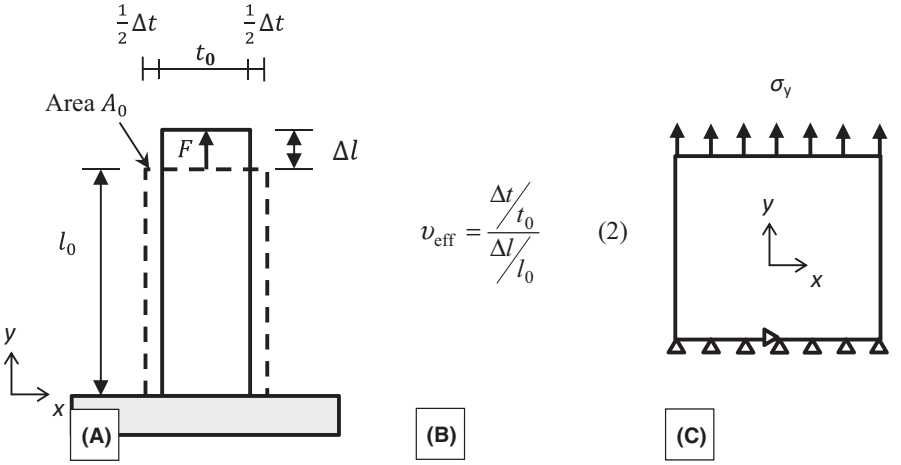

FIGURE 4 Tensile test for Poisson ratio determination (A), equation for calculation of Poisson ratio (B), and the FE model for v_{yx} and v_{yz} determination in simplified 2D illustration (C)[22]

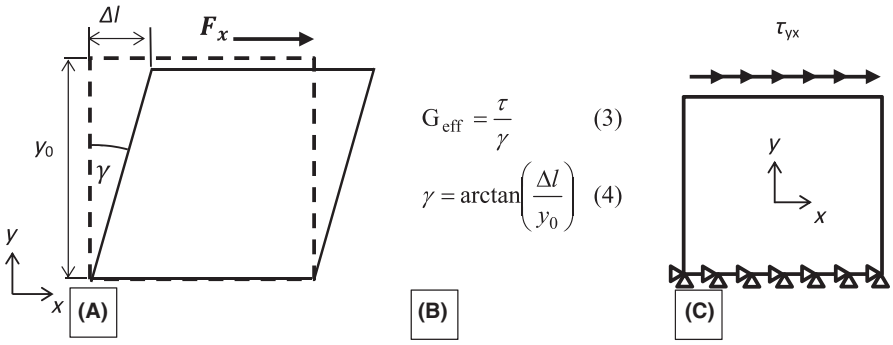

FIGURE 5 Schematic drawing of shear test (A), equations for shear modulus calculation (B), and the FE model for G_{yx} determination in simplified 2D illustration (C)[22]

3.3 | Effective shear modulus

The shear modulus is defined as the ratio of shear stress τ to elastic shear deformation angle γ (compare Equations 3 and 4 in Figure 5B). Again, the anisotropic properties of the fin structure result in six different shear moduli. Taking G_{yx} as an example, nodes at minimum y form the base, while at maximum y the shear force is applied in x-direction, which leads to a deformation angle (γ). Figure 5A illustrates a shear stress deformation in the xy-plane and the corresponding change in shear angle in the linear elastic range on the basis of a rectangle. Figure 5C shows a simplified 2D illustration of the FE model with boundary conditions for G_{yx} determination. Here, the shear force τ_{yx} acts perpendicular to the yz plane, while the basis is formed by nodes at minimum y. For G_{yz} a shear force has to act perpendicular to the yx plane. The remaining components of the shear modulus (G_{xy}, G_{xz} and G_{zx}, G_{zy}) are determined analogously.

4 | EXPERIMENTAL SETUP: SHEAR TEST

In a ceramic heat exchanger, shear stresses are more critical than compressive stresses. They are caused on the one hand by different thermal expansions within the heat exchanger and on the other hand by external forces, which are, for example, caused by press fixations. In order to ensure the reliability of the model results, experiments were carried out on a test bench and compared with model results. The aim was to demonstrate the accuracy of the developed ANSYS® model.

4.1 | Experimental setup

The main part of the test setup is a Zwick and Roell press, which can provide shear forces of maximum 200 kN. A spindle drive enables precise test speeds of 1 µm min^{-1} to 100 mm min^{-1}. The test rig is equipped with internal force and distance sensors. In order to obtain robust results, the specimen must be prevented from tilting. This is done by a sample fixation system consisting of two T-squares and bar spacers. Figure 6 illustrates the experimental setup. The sample is placed such that there is a vertical fixed bearing on the left sample leg and a vertically floating bearing on the right. The load is induced at the top of the right, not vertically fixed steel leg and acts as shear stress parallel to the fin base.

The fin samples themselves are made of aluminum and have 18 equally long fins on each fluid side. Both sides are spatially separated by a "heat exchanger plate." Figure 7A illustrates the fin structure with its geometrical dimensions. For the shear force impingement, negative forms are used. Those are made from steel. Due to its three times higher Young's modulus, compared with aluminum, distortion of the results is reduced. The forms transfer the force parallel to their base into the fins and thus cause shear deformation of the entire sample.

To improve accuracy of the results, the digital image analysis software ARAMIS®[20] is used. Therefore, the entire sample (fins and negative forms) has to be sprayed with white background color and black dots (Figure 6). ARAMIS® detects the black dots and their movement as a function of time, piston travel, and used load. The software is able to determine the deformation of the fins without considering the deformation of the negative forms.

4.2 | Experimental procedure

The sample with its negative forms is inserted into the test rig as shown in Figure 6**.** The parameters and conditions

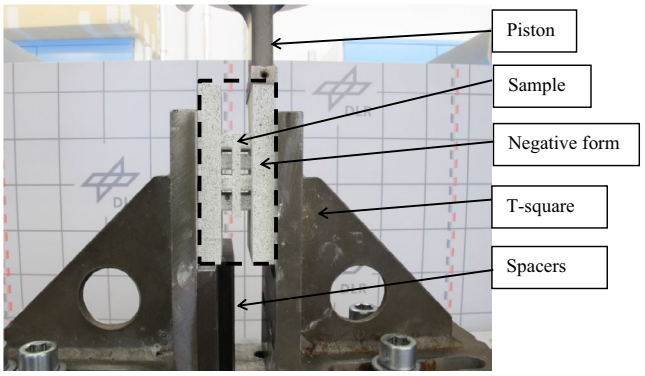

FIGURE 6 Experimental setup for shear module determination

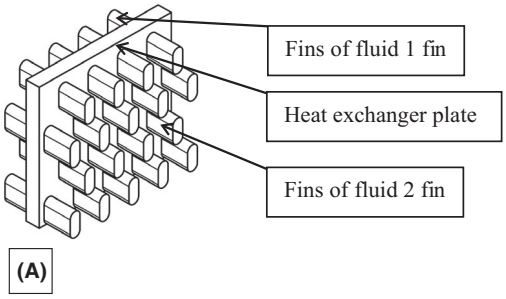

h/mm	5
s/mm	6
t/mm	3
l/ mm	7
Plate thickness/mm	4
Plate width/mm	41
Plate height/mm	38

(B)

FIGURE 7 Aluminum sample for experimentally shear modulus determination (A) and its geometrical parameters according to Figure 1B

TABLE 1 Test facility parameter

Test facility	Zwick Roell 200 kN
Test speed/mm s^{-1}	0.005
Initial load/N	25
Maximum load/N	7000
Ambient temperature/°C	21.6
Humidity/%	50

used for the experimental procedure are listed in Table 1. First, the initial load of 25 N is applied to the sample to check the fixation setup and tare the force and displacement measuring systems. Afterward, the test procedure starts. Due to the constant piston movement, the load is continuously increased to a maximum value of 7 kN. During the entire measurement, changes in distance and load are recorded. Each 500 N a digital image of the whole sample is taken. After the test procedure, the exact deformation, stress, and strain of the fins are determined by using the pictures and the ARAMIS® software. Together with Equations (3) and (4), the resulting shear moduli are calculated. For the validation, only shear moduli in one direction are determined. A total amount of ten samples are tested.

5 | RESULTS AND DISCUSSION

For each of the effective material models discussed, a domain size and mesh study were conducted. In order to demonstrate the functionality of the methodology, the effective shear model was validated. Furthermore, effective substitute material properties were determined for five different fin geometries to prove the orthotropic characteristic of the OSF plate heat exchanger core.

5.1 | Model and mesh size determination

The considered domain size of the ANSYS® models was subject to a size independence study. Taking into account, the symmetry and periodicity of the OSF HTHE-core five different sizes of the representative model domain (Figure 8) were tested to gain the best time and accuracy ratio.

Figure 9 illustrates the Young's modulus as a function f model domain size. A maximum change of 8% can be observed from domain size one to three. Thereafter, changes below 0.1% occur. The results regarding Poisson ratio and shear modulus are similar. In order to save computational time, model size number three was chosen for subsequent analysis.

A grid independence study was performed using a tetrahedral mesh. Ten different mesh sizes, listed in Table 2, were tested on the basis of the previously selected domain size. For

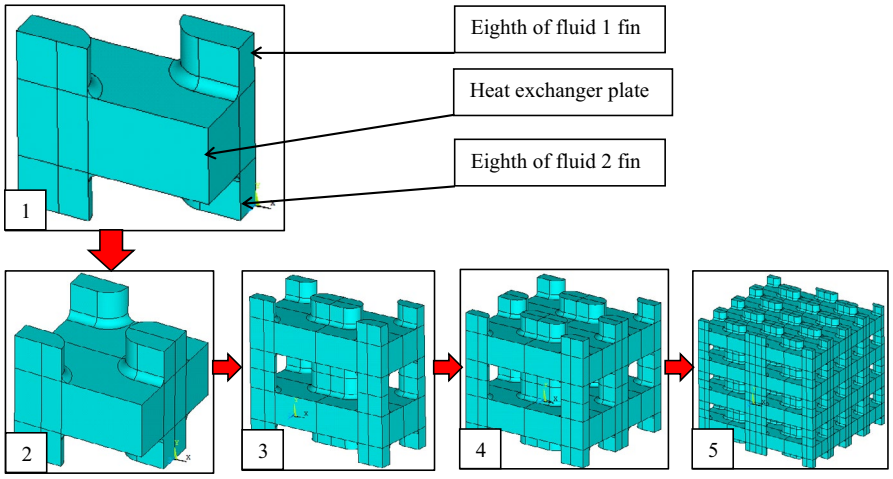

FIGURE 8 Exemplary representation of the different considered domain sizes within the domain size independent study

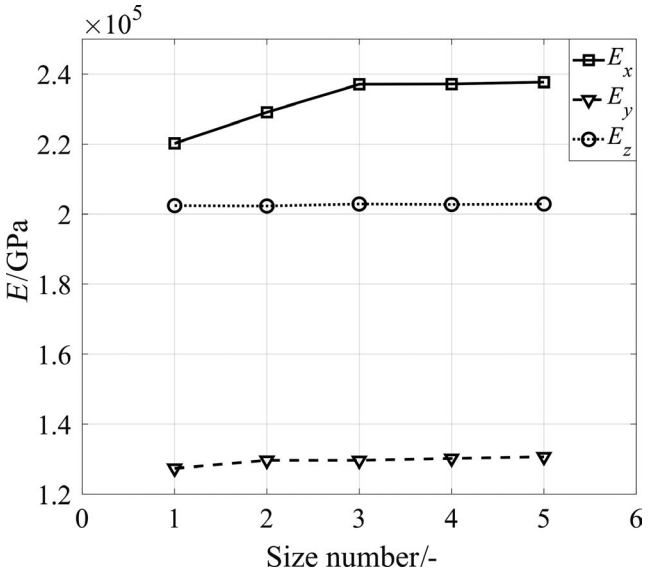

FIGURE 9 Domain size study results for the Young's modulus model

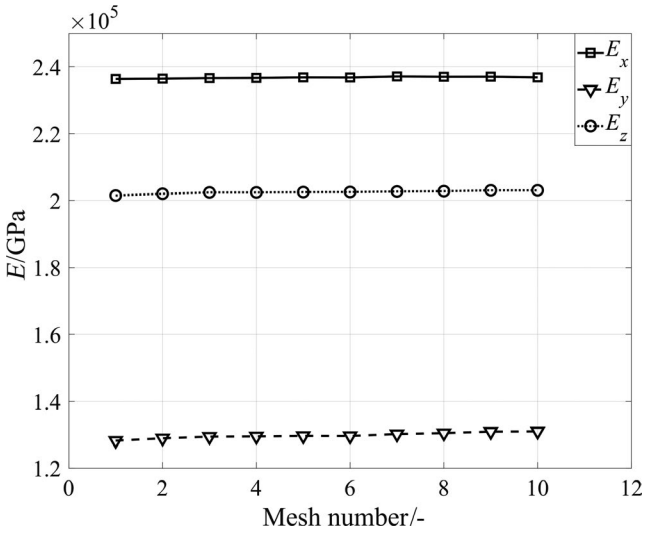

FIGURE 10 Mesh size study results for the Young's modulus model

TABLE 2 Mesh number and size

Numbers	Amount of nodes
1	135 226
2	110 781
3	79 188
4	55 247
5	44 597
6	42 987
7	31 551
8	30 235
9	28 202
10	26 651

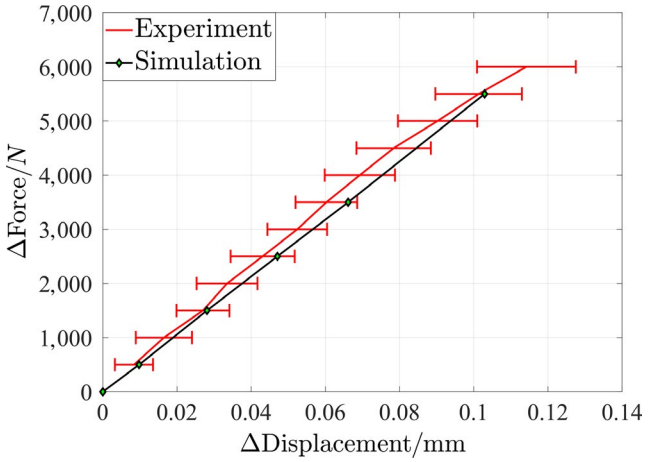

FIGURE 11 Comparison of simulation (black) vs experimentally shear test results (red)

instance, the results for the Young's modulus are depicted in Figure 10. Deviations below 0.2% between the finest and the coarsest mesh are visible. Here, too, the results for Poisson ratio and shear modulus are similar. Therefore, due to the time efficiency, mesh number nine is used for the subsequent validation and ongoing research.

5.2 | Validation of the effective shear modulus model

In order to validate the shear modulus model, simulations and experiments were performed with the geometrical fin parameter shown in Figure 7. The experiments were conducted using the presented test setup, and the results were obtained by using the digital image analysis software ARAMIS®. To reduce inaccuracy, ten samples with the same fin dimensions were tested.

Figure 11 illustrates the average experimental results with their standard deviations of the shear tests (red) compared with the simulation results shown in black. It can be seen that displacements obtained with the experimental setup agree well with the results of the simulation model. Using Equation (3) for shear modulus calculation, an averaged experimental shear modulus of 512 MPa with a standard deviation of 24 MPa can be determined. With the computational model, an effective fin shear modulus of 498 MPa is received. The maximum deviation between numerical and experimental results is 2.8%. This shows the feasibility and reliability of the effective shear modulus model.

In addition, the resulting effective shear modulus is more than fifty times smaller compared with a pure aluminum block (25.5 GPa). The same can be observed for the effective Young's modulus. Here, the value is with 21 GPa instead of 70 GPa smaller, too. This results from the porous

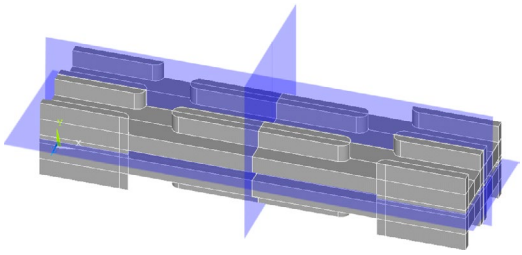

(A)

$$\begin{pmatrix}\varepsilon_{xx}\\ \varepsilon_{yy}\\ \varepsilon_{zz}\\ \varepsilon_{xy}\\ \varepsilon_{yz}\\ \varepsilon_{xz}\end{pmatrix} = \begin{pmatrix} \frac{1}{E_x} & -\frac{\nu_{xy}}{E_x} & -\frac{\nu_{xz}}{E_x} & & & \\ -\frac{\nu_{xy}}{E_x} & \frac{1}{E_y} & -\frac{\nu_{yz}}{E_y} & & & \\ -\frac{\nu_{xz}}{E_x} & -\frac{\nu_{yz}}{E_y} & \frac{1}{E_z} & & & \\ & & & 1/G_{xy} & & \\ & & & & 1/G_{yz} & \\ & & & & & 1/G_{xz} \end{pmatrix} \begin{pmatrix}\sigma_{xx}\\ \sigma_{yy}\\ \sigma_{zz}\\ \tau_{xy}\\ \tau_{yz}\\ \tau_{xz}\end{pmatrix}$$

(B)

$$\frac{\nu_{xy}}{E_x} = \frac{\nu_{yx}}{E_y} \qquad \frac{\nu_{xz}}{E_x} = \frac{\nu_{zx}}{E_z} \qquad \frac{\nu_{yz}}{E_y} = \frac{\nu_{zy}}{E_z}$$

(C)

FIGURE 12 Fin example with depicted symmetric planes (A), orthotropic stress-strain matrix (B), and equations of symmetric conditions (C)

TABLE 3 Fin geometries for effective material property are determined

Geometry numbers	*s*/mm	*t*/mm	*l*/mm	*h*/mm
1	1.00	1.00	10.00	1.00
2	3.50	1.93	24.84	2.00
3	7.50	2.44	75.00	3.00
4	10.00	5.50	55.00	4.00
5	8.50	5.00	60.00	5.00

TABLE 4 Material parameters of sintered silicon carbide

	E/GPa	*ν*/–
SSiC	410	0.17

structure of the sample and the fact that a higher degree of porosity results in higher deformations at the same stresses. Thus, the sample shows a lower Young's and shear modulus.[19]

5.3 | Proof of orthotropic material behavior

Figure 12A illustrates a symmetric OSF section. Due to the evenly distributed fins, three symmetric plates (blue squares), which are perpendicular to each other, can be marked. The geometrical dimentions (*l, h, t, s;* compare Figure 1) used for Figure 12A are examples, but can vary without changing the material behavior.

By proving the orthotropic behavior of the OSF structure model, the independent material constants—Young's modulus, Poisson ratio, and shear modulus—can be reduced to nine and thus, computational time can be saved. A material shows orthotropic behavior, if its mechanical properties behave symmetrically with respect to the symmetric plates. For orthotropic materials, however, the normal and shear components are decoupled: Normal stresses (perpendicular to a symmetric plate) only cause normal strains, and shear stresses only cause shear strains. The corresponding orthotropic stress-strain matrix is given in Figure 12B. A fundamental property of this matrix is its symmetry. This results in three symmetrical conditions of orthotropic resilience, which are shown in Figure 12C. According to these relationships, the number of independent mechanical material constants can be reduced to nine for orthotropic materials.

To show the orthotropic mechanical behavior of the fin structure model, effective material properties were determined for five different, randomly selected fin geometries and their symmetric conditions were checked. Table 3 shows the considered fin dimensions. As initial material parameters, the ones of sintered silicon carbide were used (Table 4).

The results obtained for the five geometries considered are listed in Table 5. The Young's moduli, Poisson ratios, and the equations of symmetric conditions (Figure 12C) were used to examine the stress-strain symmetry. Comparing the results, the symmetric conditions agree within a maximum deviation of 1.8%. This indicates the orthotropic behavior of the fin section model. Thus, only nine independent effective

TABLE 5 Effective Young's moduli, Poisson ratios, and symmetric test results for the fin geometries given in Table 3

	E - modulus/GPa			Poisson ratio/–						Symmetric test/$\times 10^{-7}$					
Nr	E_x	E_y	E_z	ν_{xy}	ν_{xz}	ν_{yx}	ν_{yz}	ν_{zx}	ν_{zy}	$\frac{\nu_{xy}}{E_x}$	$\frac{\nu_{yx}}{E_y}$	$\frac{\nu_{xz}}{E_x}$	$\frac{\nu_{zx}}{E_z}$	$\frac{\nu_{yz}}{E_y}$	$\frac{\nu_{zy}}{E_z}$
1	346	268	302	0.165	0.169	0.130	0.134	0.147	0.149	4.77	4.84	4.88	4.87	5.00	4.93
2	281	170	231	0.162	0.170	0.099	0.089	0.140	0.120	5.78	5.83	6.05	6.06	5.24	5.19
3	231	118	185	0.164	0.170	0.084	0.058	0.137	0.090	7.09	7.13	7.36	7.40	4.92	4.86
4	227	158	170	0.152	0.172	0.106	0.074	0.129	0.080	6.69	6.70	7.58	7.59	4.68	4.71
5	216	165	146	0.150	0.171	0.115	0.079	0.116	0.070	6.96	6.97	7.92	7.95	7.79	4.79

substitute material properties—E_x, E_y, E_z, v_{xy}, v_{xy}, v_{xy}, G_{xy}, G_{yz}, and G_{xz}—are required to characterize the entire substitute model.

6 | SUMMARY AND CONCLUSION

In this work, a novel thermomechanical simulation methodology for a time-saving identification of mechanically stable ceramic plate-fin heat exchanger arrangements is presented. It is based on the OSF plate fin structure, which is already subject to ceramic heat exchanger research. The structure shows a large number of fins and numerous geometrical degrees of freedom; which is why detailed thermomechanical design simulations of different fin dimensions are usually associated with high computational effort. The methodology presented, which is based on a homogenized substitute heat exchanger model, reduces this effort.

The methodology requires effective substitute material properties that are required, consisting of the effective Young's modulus E, effective shear modulus G, and effective Poisson ratio v. In order to determine these properties, three simulation models were developed and presented which are based on the standardized test procedures of the German Industrial Standard (DIN).

By means of a model domain and mesh size independence study, both a computationally time-saving model size and mesh size could be identified. In order to ensure the accuracy of the model results, the shear modulus model was validated. For this purpose, a special test rig was set up to experimentally determine the shear modulus of ten identical samples. The experimental results were compared with the simulation results finding a maximum deviation of less than 3%. Furthermore, the material behavior of the fin structure was investigated with respect to the orthotropic stress-strain relation. With an agreement of 98.2% between the symmetric orthotropic relationships, the orthotropic material property of the fin structure was demonstrated. This reduces the number of independent effective material properties to nine and thus leads to a reduced computational time.

The presented work sets the basis for detailed time-saving thermomechanical design studies of plate-fin heat exchangers. Future work will focus on the setup of the whole thermomechanical design model including the substitute model, the impingement of boundary conditions, extraction of critical displacements, and their implementation into a small fin section for thermomechanical stress calculation.

NOMENCLATURE

A	area/m^2
E_{eff}	effective Young's modulus/Pa
F	force/N
G_{eff}	effective shear modulus/Pa
h	fin height/m
l	fin length/m
l_0	original length/m
Δl	change in length/m
s	lateral fin spacing/m
t	fin thickness/m
Δt	change in thickness/m
v_{eff}	effective Poisson ratio/–

GREEK SYMBOLS

γ	deformation angle/rad
τ	shear stress/N m^{-2}

ORCID

Jürgen Haunstetter https://orcid.org/0000-0003-0212-3592

REFERENCES

1. Kautz M, Hansen U. The externally-fired gas-turbine (EFGT-Cycle) for decentralized use of biomass. *Appl Energy*. 2007;84(7-8):795-805.
2. Folke C, Romey I. Efficiencies of integrated gasification combined cycle power stations with chemical quench. In: *5th International Conference on Technologies and Combustion for a Clean Environment, Lisbon*; 1999:779-784.
3. Al-attab KA, Zainal ZA. Externally fired gas turbine technology: a review. *Appl Energy*. 2015;138:474-487.
4. Sommers A, Wang Q, Han X, T'Joen C Park Y, Jacobi A. Ceramics and ceramic matrix composites for heat exchangers in advanced thermal systems a review. *Appl Therm Eng*. 2010;30:1277-1291.
5. Shi H-N, Ma T, Chu W-X, Wang Q-W. Optimization of inlet part of a microchannel ceramic heat exchanger using surrogate model coupled with genetic algorithm. *Energy*. 2017;149:988-996.
6. Alm B, Imke U, Knitter R, Knitter R, Schygulla U, Zimmermann S. Testing and simulation of ceramic micro heat exchangers. *Chem Eng J*. 2008;135:179-184.
7. Kee RJ, Almand BB, Blasi JM, et al. The design, fabrication, and evaluation of a ceramic counter-flow microchannel heat exchanger. *Appl Therm Eng*. 2011;31:2004-2012.
8. Schulte-Fischedick J, Dreißigacker V, Tamme R. An innovative ceramic high temperature plate-fin heat exchanger for EFCC processes. *Appl Therm Eng*. 2007;27(8-9):1285-1294.
9. Haunstetter J, Dreißigacker V, Zunft S. Ceramic high temperature plate fin heat exchanger: experimental investigation under high temperatures and pressures. *Appl Therm Eng*. 2019;151:364-372.
10. de Mello P, Scuotto S, Ortega F, Donato G. Heat transfer and pressure drop in a plate and fin ceramic heat exchanger. In: *Conference on Experimental Heat Transfer, Fluid Mechanics and Thermodynamics*; 2013:16-20.
11. Monteiro D, de Mello P. Thermal performance and pressure drop in a ceramic heat exchanger evaluated using CFD simulations. *Energy*. 2012;45(1):489-496.
12. Villanueva H, de Mello P. Heat transfer and pressure drop correlations for finned plate ceramic heat exchangers. *Energy*. 2015;88:118-125.

13. Chiappini G, Sasso M, Bellezze T, Amodio D. Thermo-structural analysis of components in ceramic material. *Struct Integrity Procedia*. 2018;8:618-627.
14. Nemeth N, Jadaan O, Gyekenyesi J. *Lifetime reliability prediction of ceramic structures under transient thermomechnical loads*, NASA/TP, 2005–212505.
15. Rolfes R, Noack J, Taeschner M. High performance 3D-analysis of thermo-mechanically loaded composite structures. *Compos Struct*. 1999;46:367-379.
16. DeHoff P, Barrett A, Lee R, Anusavice K. Thermal compatibility of dental ceramic systems using cylindrical and spherical geometries. *Dental Mater*. 2008;24:744-752.
17. Smyth R. A proposal for the use of a very high temperature ceramic heat exchanger in gas turbine power production. Article No. 97088. In: *Energy Conversion Engineering Conference*; 1997;1696-1701.
18. Schulte-Fischedick J, Zunft S, Streuber C. Development of a ceramic plate-fin heat exchanger for operation temperatures up to 1250°C. In: *Sixth International Conference on Enhanced, Compact and Ultra-compact Heat Exchangers*; 2005.
19. Kováčik J. Correlation between Young's modulus and porosity in porous materials. *J Mater Sci Lett*. 1999;18:1007-1010.
20. *Aramis professional software*. https://www.gom.com/3d-software/gom-system-software/aramis-professional.html. Homepage of GOM precise industrial 3D metrology. Accessed October 22, 2018.
21. Manglik RM, Bergles AE. Heat transfer and pressure drop correlations for the rectangular offset strip fin compact heat exchanger. *Exp Thermal Fluid Sci*. 1995;10(2):171-180.
22. Roylance D. *Mechanical properties of materials. Course book MIT*; 2008.

How to cite this article: Haunstetter J, Dreißigacker V. Ceramic high temperature plate-fin heat exchanger: A novel methodology for thermomechanical design investigation. *Energy Sci Eng*. 2019;00:1–10. https://doi.org/10.1002/ese3.502